Korean J. Chem. Eng., 36(7), 1193-1200 (2019)
DOI: 10.1007/s11814-019-0293-z

pISSN: 0256-1115
eISSN: 1975-7220

AgNi@ZnO nanorods grown on graphene as an anodic catalyst for direct glucose fuel cells

Thoa Thi Kim Huynh*,‡, Thao Quynh Ngan Tran,‡, Hyon Hee Yoon*, Woo-Jae Kim***,†, and Il Tae Kim*,†**

*Department of Chemical and Biological Engineering, Gachon University, Seongnam-si, Gyeonggi-do 13120, Korea
**Department of Machine and Equipment, Faculty of Chemical Engineering,
Industrial University of Ho Chi Minh City, No 12 Nguyen Van Bao, Go Vap, HCMC, Vietnam
***Department of Chemical Engineering and Materials Science, Ewha Womans University, Seoul 03760, Korea
(*Received 12 March 2019 • accepted 7 May 2019*)

Abstract−Nano carbon-semiconductor hybrid materials such as graphene and zinc oxide (ZnO) have been vigorously explored for their direct electron transfer properties and high specific surface areas. We fabricated a three-dimensional anodic electrode catalyst nanostructure for a direct glucose fuel cell (DGFC) utilizing two-dimensional monolayer graphene and one-dimensional ZnO nanorods, which accommodate silver/nickel (Ag/Ni) nanoparticle catalyst. Glucose, as an unlimited and safe natural energy resource, has become the most popular fuel for energy storage. Ag and Ni nanoparticles, having superior catalytic activities and anti-poisoning effect, respectively, demonstrate a 73-times enhanced cell performance (550 μW cm^{-2} or 8 mW mg^{-1}) when deposited on zinc oxide nanorods with a small amount of ~0.069 mg in 0.5 M of glucose and 1 M of KOH solution at 60 °C. This three-dimensional anodic electrode catalyst nanostructure presents promise to open up a new generation of fuel cells with non-Pt, low mass loading of catalyst, and 3D nanostructure electrodes for high electrochemical performances.

Keywords: 3D Nanostructures, CVD Graphene, Direct Glucose Fuel Cell, Nickel Nanoparticles, Silver Nanoparticles, Zinc Oxide Nanorods

INTRODUCTION

Renewable energy resources have gained great attention for developing future viable energy technology owing to global energy consumption growth and environmental issues. Glucose obtained from the abundant residual biomass produced by the agriculture and/or humanity activities has been considered as a viable resource in order to obtain useful energy [1,2]. In addition, glucose can generate an energy of 2.87×10^6 J mol^{-1} by completely converting into CO_2 with 24 electron transfers, implying a comparable energy efficiency with alcohol fuels such as ethanol and methanol [3,4]. Currently, glucose has been exploited as a potential fuel in applications for enzymatic and direct fuel cells. Enzymatic fuel cells utilizing glucose oxidation [5] and glucose dehydrogenase [6] have shown a power density of 1.45 mW cm^{-2} [7]. However, they display limited lifetimes (7-10 days). As a result, direct glucose fuel cells have been more attractive in improving cell performance and developing low cost systems [8]. To overcome the aforementioned difficulties related to shortened lifetimes, new approaches have been explored. Among these, direct glucose fuel cells using a metallic catalyst and an alkaline medium have opened a new vision for energy systems.

For several decades, noble metals with outstanding catalytic activity and high stability were employed as electrode materials for non-bio-glucose fuel cells [9,10]. To date, some reported electrical power outputs have been performed using several direct glucose fuel cell (DGFC) types [5,7,11-15]. It has been observed that glucose fuel cells demonstrate higher performance with anion exchange membrane fuel cells (AEMFC), using precious metal-based electrode catalysts such as Pt, Au, and their alloys [16,17]. In particular, Basu et al. tried to develop a bimetallic catalyst, Pt-Pd, and a trimetallic catalyst, Pt-Pd-Au, for anode electrode in DGFC, using which a power density of 0.52 mW cm^{-2} was obtained in 0.3 M of glucose and 1 M of KOH aqueous medium [11]. Currently, some investigations on non-Pt metals and their alloys with Ni [5], Co [18], and Pd [12] have been studied in an effort to reduce the high cost and to improve the efficiency of DGFC. Among the nonprecious metal alloys, nickel is an excellent candidate for glucose oxidation reactions in alkaline media as well [5,18-22]. Gao et al. reported that Ni-Co cocatalyst shows a performance of 23.97 W m^{-2} at room temperature for direct glucose alkaline fuel cell (DGAFC) [22]. Yang et al. [8] applied Ni foams as electrocatalysts with methyl viologen as an electron mediator for DGFC and achieved a power density of 5.20 W m^{-2} in 1 M of glucose and 3 M of KOH medium at room temperature. In addition, silver with great electrocatalytic property in alkaline media has been used in glucose substrate. Chen et al. applied a support of nickel foam in silver particles to obtain a cell performance of 2.03 mW cm^{-2} at 80 °C [23]. Consequently, many researchers have focused on metallic components to improve DGFC performance, reduce cost, and increase catalytic activities and stabilities. Based on the research trend, new anodic generations with nanostructure in various dimensions are considered promising for

†To whom correspondence should be addressed.
E-mail: wjkim1974@ewha.ac.kr, itkim@gachon.ac.kr
‡T. T. K. Huynh and T. Q. N. Tran contributed equally to this work.

the DGFC field. Graphene with its two-dimensional carbonaceous structure has been widely applied in sensors [24-26], supercapacitors [26-29], catalysts [30-32], electronics, transistors, photonics, and optoelectronics [29] owing to its outstanding electrical conductivity, large specific surface area, mechanical strength, chemical stability, and great optical properties [7]. Its appeal is further increased by the fact that it possesses a great mobility of 200 000 $cm^2 V^{-1} s^{-1}$ [33,34] and a surface-to-mass ratio of 2,600 $m^2 g^{-1}$ [27]. Monolayer graphene synthesized via chemical vapor deposition (CVD) has displayed some excellent properties that are required to improve catalytic activities. Recently, Qu et al. replaced Pt/C electrode by N-doped graphene synthesized via CVD for alkaline fuel cells, resulting in long-term stability and decreased poison effect [35]. A typical revolution in this work is the 3D construction of ZnO aligned nanorods (NRs) on a single layer graphene-covered electrolyte membrane as a preparation for decorating catalysts. ZnO is an outstanding semiconductor material. Chen et al. investigated ZnO as an electrolyte for solid oxide fuel cells at a low operating temperature, delivering a maximum performance of 864 mW cm^{-2} at 550 °C [36,37]. In addition, Wenbin et al. studied the composite of CuO-ZnO-SDC ($Sm_xCe_yO_z$) as an anodic material for direct carbon fuel cells, yielding a largest power density of 130 mW cm^{-2} at 700 °C [38]. Therefore, the recent development of the 3D nanostructured combination between ZnO nanorods and graphene film is a technical breakthrough to achieve higher performance in DGFC due to its significant surface area, stability, and increased catalytic activity [5,7,20].

In this work, we aimed to support the catalytic effect by applying a 1D nanomaterial such as ZnO nanorods to improve the cell performance. In particular, a bimetallic Ag-Ni catalyst was anchored on the 3D nanostructure consisting of 1D ZnO NRs and CVD single layer graphene film. The 3D nanostructure acting as an accommodation for nanoparticle catalysts enhanced the electrochemical catalytic reaction, thereby demonstrating good electrochemical performances.

EXPERIMENT

1. Chemicals and Materials

Ammonium persulfate [$(NH_4)_2S_2O_8$], poly(methyl methacrylate) (PMMA), zinc acetate $Zn(CH_3COO)_2$, zinc nitrate hexahydrate [$Zn(NO_3)_2{\cdot}6H_2O$], hexamethylenetetramine (HTMA, $C_6H_{12}O_4$), silver nitrate ($AgNO_3$), nickel nitrate hexahydrate [$Ni(NO_3)_2{\cdot}6H_2O$], and sodium borohydride ($NaBH_4$) were purchased from Sigma Aldrich in Korea. All chemical materials were used without any further purification. Copper foil was distributed by Alfa Aesar with the grade of graphene synthesis, and the anion exchange membrane (FAA-130 electrolyte membrane) was supplied by FuelcellStore.

2. Synthesis of Material

2-1. Preparation of ZnO Nanorods on Monolayer Graphene

For synthesizing monolayer graphene, copper foil (Alfa Aesar, 25 μm thick, 99.8%) was used to synthesize graphene by employing the chemical vapor deposition method at 1,020 °C in vacuum atmosphere. First, Cu foil was cleaned using a diluted aqueous 1 wt% of HNO_3, followed by several cleaning steps with deionized water (DI water), isopropyl alcohol (IPA), and acetone. A cuvette-shaped inner tube with an outer diameter of 4 mm was inserted into the quartz tube of CVD system in the direction of gas flow. A movable furnace was heated to 1,020 °C for 1.5 h under the flow of Ar gas during the pregrowth step. During the second step that includes the annealing and growth process, the annealing stage took 2 h in the mixture of 100 sccm Ar and 100 sccm H_2 at pressure of 0.6 mtorr, and then (1-20) sccm CH_4 gas flow was introduced for the growth stage at 1,020 °C. Subsequently, the whole system was cooled down rapidly to ambient temperature in Ar environment. Next, the graphene-grown Cu foil was covered with PMMA using spin coating before removing Cu with the etchant solution of ammonium persulfate. Finally, graphene was transferred on a polymer substrate (anion exchange membrane) for next steps, and PMMA was removed using the acetone solution.

To grow ZnO nanorods on graphene, 0.0459 g of zinc acetate was dispersed in 30 ml of C_2H_5OH using ultrasonication, and then it was spin cast on graphene-transferred polymer several times at 3,000 rpm, followed by annealing at 80 °C for each coating. Second, the polymer was dipped into a mixture of 10 ml of HTMA (50 mM) and 10 ml of Zn $(NO_3)_2{\cdot}6H_2O$ (50 mM) at pH 13. This experiment was carried out at 90 °C in a heating bath for 1 h. Lastly, zinc oxide nanorods was rinsed with DI water for three times to obtain a clear surface, and then it was dried for next steps.

2-2. Decoration of Ag and Ni Nanoparticles on ZnO NRs

The Ag-Ni bimetallic nanoparticle catalyst was anchored on ZnO nanorods-graphene substrate from the precursors of $AgNO_3$ and $Ni(NO_3)_2{\cdot}6H_2O$ aqueous solution with different mole ratios as listed in Table 1.

The precursor mixtures were dispersed into 10 ml of C_2H_5OH using the ultrasonication process for 30 min. Since Ag is highly photosensitive, it is essential for the sample to be prepared in dark condition during this step and to obtain pure metallic catalyst. Thus, the sample was baked on a hot plate at 80 °C in aforementioned condition after each time the above-mentioned salt mixtures were covered onto the surface of ZnO nanorods grown on graphene/polymer membrane. Next, this sample was dipped vertically into a beaker containing 100 ml of $NaBH_4$ solution under the support of ice bath (3 °C), and maintained reaction for 5 min before pressing into the membrane electrolyte assembly (MEA) for the implementation of fuel cell. To investigate the role of ZnO nanorods, a mixture of 0.013 g of $AgNO_3$ and 0.022 g of $Ni(NO_3)_2{\cdot}6H_2O$ in ethanol was sequentially covered on carbon paper and on graphene/membrane, and then the aforementioned experimental steps were followed. Overall scheme for the preparation of 3D nanostructure catalysts is shown in Fig. 1.

3. Glucose Fuel Cell Construction

Glucose fuel cell unit was designed using metal-based anode

Table 1. Different ratios of salts for the preparation of catalyst material

Samples	Composition of precursor
Sample 1	0.022 g of $Ni(NO_3)_2{\cdot}6H_2O$
Sample 2	0.013 g of $AgNO_3$+0.022 g of $Ni(NO_3)_2{\cdot}6H_2O$
Sample 3	0.013 g of $AgNO_3$+0.11 g of $Ni(NO_3)_2{\cdot}6H_2O$
Sample 4	0.065 g of $AgNO_3$+0.022 g of $Ni(NO_3)_2{\cdot}6H_2O$
Sample 5	0.013 g of $AgNO_3$

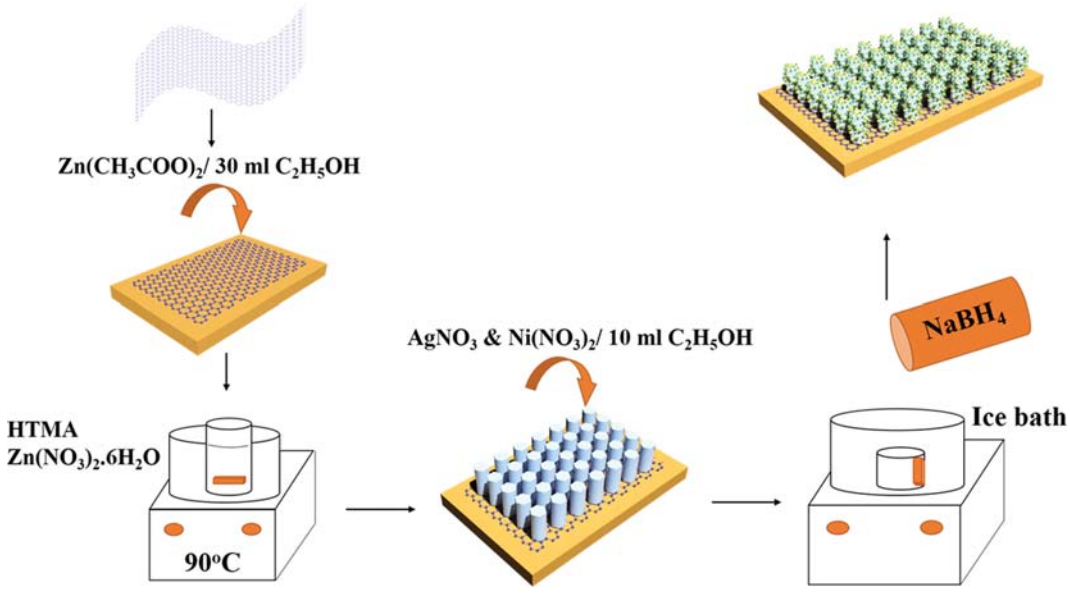

Fig. 1. Schematic for the synthesis of 3D nanostructure catalysts.

and cathode. The Ag/Ni anchored on ZnO nanorods, grown on monolayer graphene, was directly prepared on anion exchange membrane (AEM) as nanosheets for the anode side. Ionomer was used as the binder for hydroxyl conductivity in anode side. Commercial Pt/C was used in cathode side, and the AEM electrolyte was fixed between the anode and cathode compartments. Two graphite plates, including two channels for providing fuels and AEM, were fixed as the sandwich structure to form a glucose-based fuel unit device. The external circuit collected from the sandwich layer passed through gold plates. The anode and cathode compartments had working area of 1 cm^2 each. These channels served with wet air at cathode, and with glucose in alkaline media at anode, respectively. There were two aluminum layers covering outside, which were fixed with the sandwich layer using several fastening parts such as bolts, washers, and nuts, ensuring that a tightly sealed electrolyte and good electrical contacts were obtained.

4. Analytical Method

Monolayer graphene synthesized using the CVD system (Scientific engineering, Suwon, South Korea) was investigated by Raman spectroscopy (DXR, Thermo Fisher Scientific, MA, USA) at wavelength of 532 nm^{-1} and combining it with the atomic force microscopy, XE-100 PSIA (Veeco, Santa Barbara, CA, USA), to analyze surface images and thickness of graphene sheet. The morphology of materials and particle sizes were determined by scanning electron microscopy (SEM, S-4700, Hitachi, Japan), and the energy dispersive X-ray spectroscopy (EDS, EX250, Horiba, Japan) characterized the composition of materials. Transmission electron microscopy (Tecani G^2 F30, FEI, Hillsboro, OR, USA) was used to determine the presence of ZnO nanorods after electrochemical reactions in the fuel cell unit device. An inductively coupled plasma (ICP) method including ICP-OES analysis, (iCAP 6000 Series, Thermo Fisher Scientific, MA, USA) and AAS analysis, (iCE 3000 Series, Thermo Fisher Scientific, MA, USA) was used to test the content of catalyst elements.

RESULTS AND DISCUSSION

1. Characterization

A CVD system was set up at 1,020 °C based on the previously reported method [39], as shown in Fig. S1 in supporting informa-

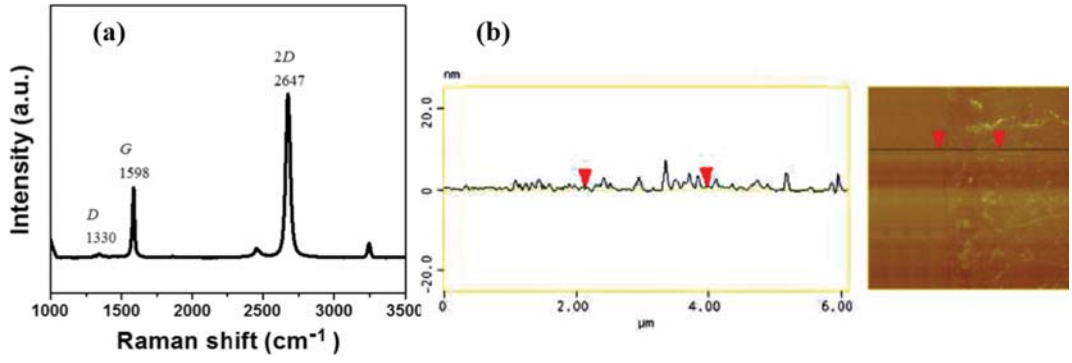

Fig. 2. (a) Raman spectrum and (b) AFM image of as-prepared graphene.

tion. As illustrated in the previous work [40], the pre-cleaning process is essential for the growth of the high quality monolayer graphene. The existence of undesired elements leads to the formation of a significant amount of nucleation sites attributing to generate graphene film with small grain sizes and the formation of island bilayer and trilayers. During the cleaning step, diluted HNO_3 (1 wt%) was used to remove contaminants from the surface of Cu foil, and further deep cleaning steps were carried out using DI water, isopropyl alcohol (IPA), and acetone with sonication for 5 min each time. This step generated the reasonable roughness on the surface of Cu, and thus it is important to perform the annealing process at high temperature under H_2 for etching that smoothly flattens the surface of Cu. Graphene grown via the CVD system on Cu foil was transferred on a Si/SiO_2 substrate and analyzed using Raman spectroscopy and AFM. In Fig. 2(a), the Raman spectrum shows a 2D/G peak ratio of 2.09 (2<2D/G<5) [41-45], which indicates that the grown graphene is monolayer. In addition, the Raman spectrum shows a very weak intensity of D band (at 1,350 cm^{-1}), illustrating the absence of defects. The thickness of film is ~0.427 nm, as shown in Fig. 2(b), which confirms the single layer graphene.

The monolayer graphene was transferred onto an anion electrolyte membrane to prepare ZnO nanorods growth in solution [46]. At first, Zn $(CH_3COO)_2$/EtOH was covered on a graphene film using the spin coating technique to form a precursor layer for planting rods. The mixture solution of Zn $(NO_3)_2 \cdot 6H_2O$ and HTMA act as nutrient sources for the growth of ZnO nanorods. Fig. 3(a) shows that, for the sample with only polymer membrane, vertically aligned ZnO-nanorods are not found on its surface even though numerous rods deposited from solution are assembled on the surface randomly. On the other hand, Fig. 3(c) clearly shows the presence of forest ZnO nanorods on the graphene-covered membrane. This result is completely consistent with the foregoing work [47] that pointed out the absence of ZnO nanorods on a bare-graphene wafer substrate. Note that the graphene sheet functions as a template [48] and contributes as a growth matrix for the synthesis of ZnO nanorods.

The anode was prepared by decorating catalyst nanoparticles on ZnO rods grown uniformly (Fig. 3(c)). Salt molecules of $AgNO_3$ and $Ni(NO_3)_2$ were stuck up for nanorods and graphene sheet. A required amount of synthesized particles of small sizes were anchored

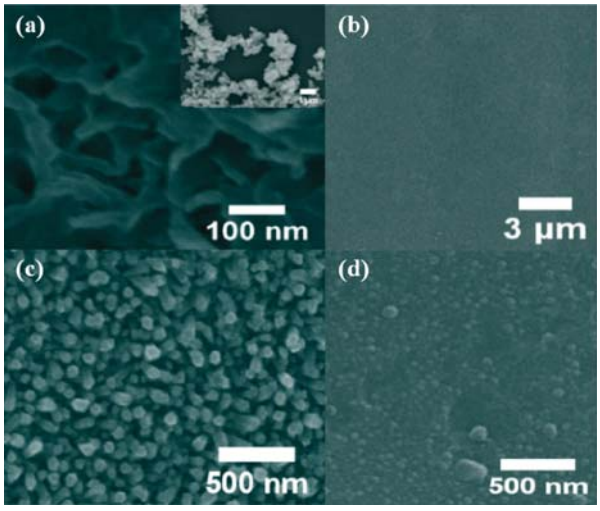

Fig. 3. SEM images of (a) prepared polymer membrane without graphene film, (b) graphene film on polymer membrane, (c) vertically aligned ZnO nanorods on graphene-polymer membrane, and (d) AgNi@nanorods grown-graphene on polymer membrane.

on the ZnO rod forest, which could be due to the prevention of the seed coalescence and Ostwald ripening phenomena that can occur in solution. As shown in Fig. 3(d), the particle size seems to be uniform, and they exist both on surface and free spaces between ZnO nanorods. To clearly prove the presence of components, EDS data analysis was performed, as shown in Fig. 4, in which the content of Ag (6.80%), Ni (4.62%), Zn (7.65%), O (20.60%), and C (53.25%) was obtained.

It is noted that potassium hydroxyl solution in fuel flow can dissolve ZnO forest on membrane. Consequently, the 3D structural design is capable of disappearing and leaving the aggregation of nanoparticles into larger ones. However, TEM images in Figs. 5(a) and 5(b), which were obtained after finishing electrochemical process for several hours, show that ZnO nanorods are retained on the membrane surface. A previous report of Ching et al. [49] revealed that ZnO nanorods synthesized in a nutrient solution with high pH level (pH=13) were not etched by alkaline solution.

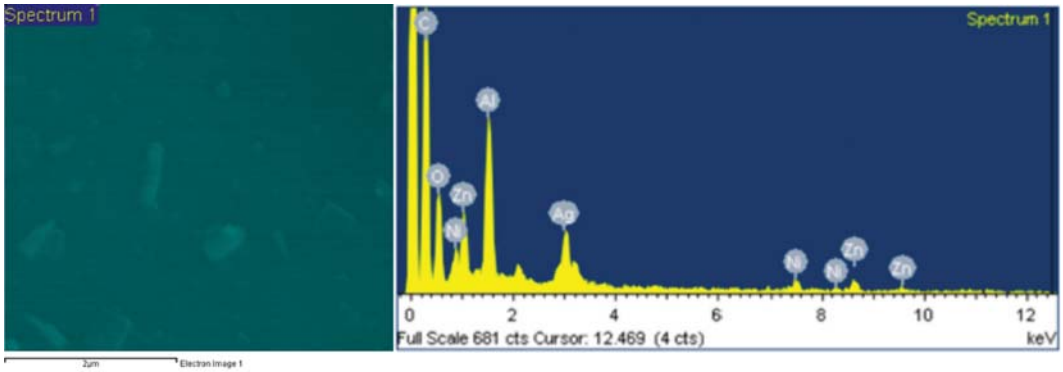

Weight %	C:O:Al:Ni:Zn:Ag = 53.25 : 20.60 : 7.08 : 4.62 : 7.65 : 6.80
Atomic %	C:O:Al:Ni:Zn:Ag = 71.02 : 20.63 : 4.20 : 1.26 : 1.87 : 1.01

Fig. 4. EDS data of AgNi@ nanorods grown graphene sample.

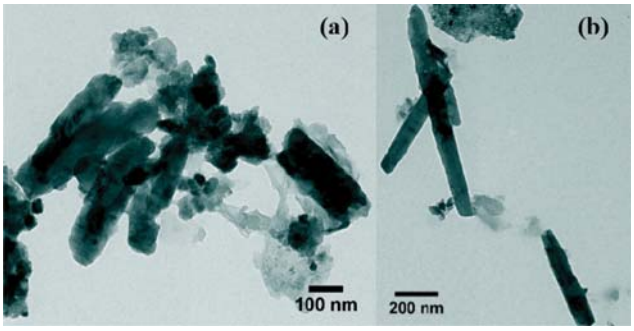

Fig. 5. (a) and (b) TEM images of ZnO nanorods existing on polymer membrane after electrochemical reactions.

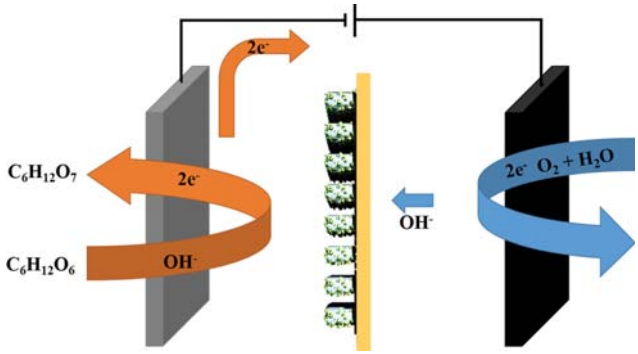

Fig. 6. Schematic of electrochemical reaction process in fuel cell unit.

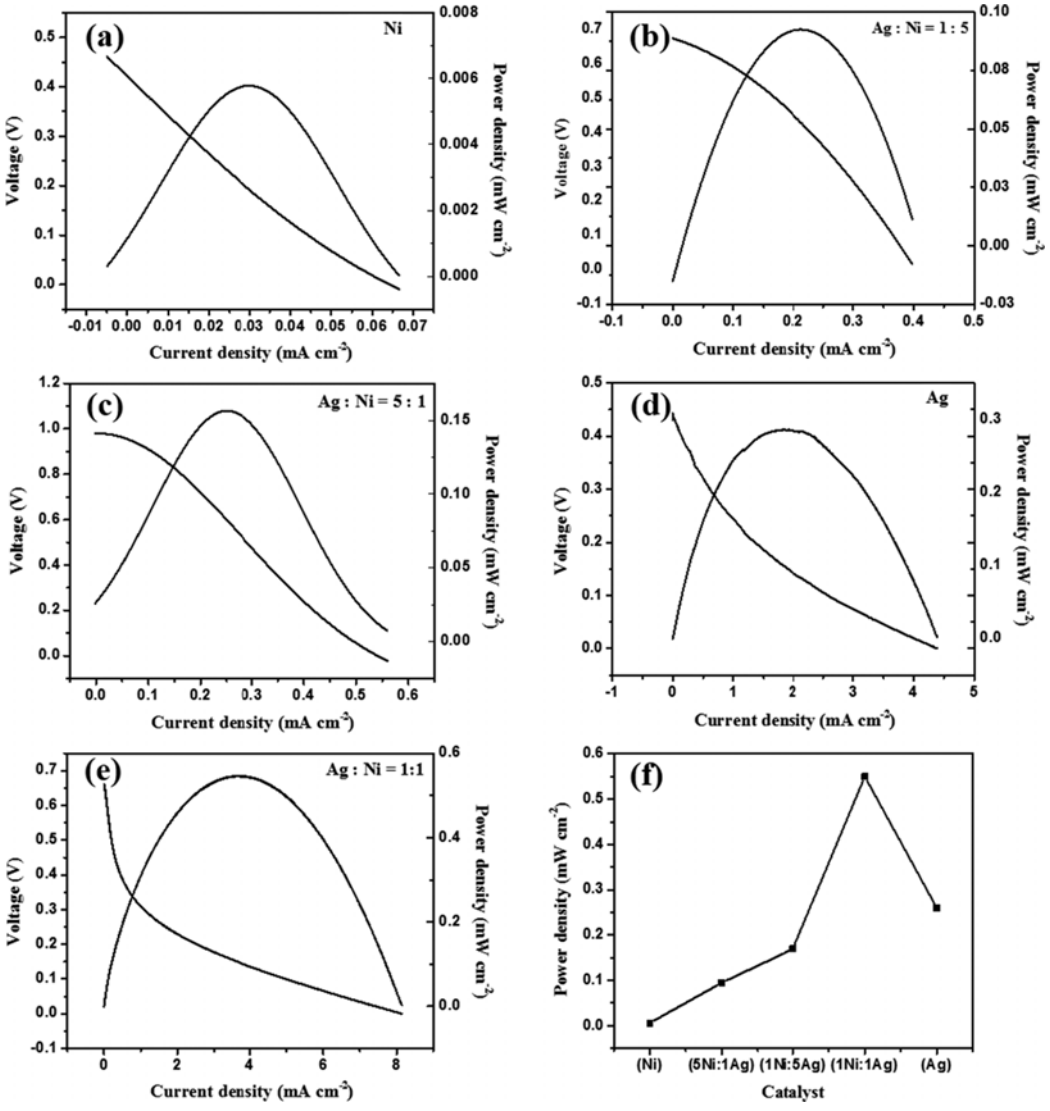

Fig. 7. Electrochemical performance of glucose unit cell in 0.5 M glucose and 1 M KOH at operating temperature of 60 °C of (a) Ni, (b) Ag : Ni (1 : 5), (c) Ag : Ni (5 : 1), (d) Ag, and (e) Ag : Ni (1 : 1) deposited on ZnO rod/graphene membrane. (f) the comparison of power densities with several catalyst systems.

2. Glucose Fuel Cell Performance

2-1. Mechanism of Glucose Fuel Cell

The as-prepared nanosheet materials were used as electrocatalytic electrodes for the glucose fuel cell. The electro-oxidation of glucose in silver electrode was conducted in the previous report [23]. Chen et al. has already elucidated the clear mechanism of a glu-

cose fuel cell in an alkaline media with a silver electrode [23]. In addition, nickel-based catalyst for glucose electro-oxidation in an alkaline media was studied by Fleischmann et al. [50,51], and the catalytic process occurred as a transformation of Ni $(OH)_2$/NiOOH. A previous study indicated that nickel oxide-modified electrodes can catalyze the electro-oxidation of glucose to gluconolactone [52] due to the existence of Ni (II) ions. The Pt/C cathode was applied to obtain the oxygen oxidation reaction with wet air. In this case, the anodic reaction can be generated with two types of mechanism as follows:

Mechanism 1:

$$Ag_2O \rightarrow 2AgO + 2e^- \quad (1)$$

$$2AgO + \text{glucose} \rightarrow Ag_2O + \text{glucolactone} \quad (2)$$

$$Ag_2O + \text{glucolactone} \rightarrow 2Ag + \text{gluconic acid} \quad (3)$$

Mechanism 2:

$$Ni(OH)_2 \leftrightarrow \beta\text{-NiOOH} + H^+ + e^- \quad (4)$$

$$Ni(OH)_2 + OH^- \leftrightarrow \gamma\text{-NiOOH} + H_2O + e^- \quad (5)$$

$$NiOOH + \text{Glucose} \leftrightarrow Ni(OH)_2 + \text{Gluconolactone} \quad (6)$$

Overall anode reaction:

$$C_6H_{12}O_6\ (\text{glucose}) + 2OH^- \rightarrow C_6H_{12}O_7\ (\text{gluconic acid}) + H_2O + 2e^- \quad (7)$$

Cathode:

$$\tfrac{1}{2}\ O_2 + H_2O + 2e^- \rightarrow 2OH^- \quad (8)$$

Overall reaction:

$$C_6H_{12}O_6\ (\text{glucose}) + \tfrac{1}{2}\ O_2 \rightarrow C_6H_{12}O_7\ (\text{gluconic acid}) \quad (9)$$

2-2. Effect of Catalyst

The electrolytic performance was studied on Ni@rod grown graphene, Ag@rod grown graphene, AgNi@rod grown graphene with the different mole ratios, 1 : 1, 1 : 5, and 5 : 1, of Ag and Ni, as shown in Fig. 7.

In overall, Ag : Ni (1 : 1)@rod grown on graphene demonstrated the most improved power density, whereas the worst was demonstrated by the cell unit of Ni@rod grown on graphene showing the power density of 0.006 mW cm^{-2}. This result was also explained with a report from Zhao et al. [53], which revealed that Ni was a poor catalyst with non-poisoning effect. In this work, the catalyst was built up directly on the electrolyte membrane, and therefore, the increase in catalyst loading declined the cell performance due to the ohmic loss. Figs. 7(b) and 7(c) show that the changes in catalyst loading from 1 : 1 to 1 : 5 (Ag : Ni) and 5 : 1 (Ag : Ni) result in the worse performance. Particularly, the power densities of 5 : 1 and 1 : 5 samples are 0.09 mW cm^{-2} and 0.16 mW cm^{-2}; even their power densities are much lower than that of Ag@rod grown graphene (0.28 mW cm^{-2}). The cooperation between Ag and Ni (1 : 1) (Fig. 7(e) and 7(f)) generated a dramatically enhanced improvement by 90 times from 0.006 mW cm^{-2} to 0.55 mW cm^{-2} compared to Ni@rod grown on graphene (Fig. 7(a)), and by two times when compared to only Ag-based fuel cell (Fig. 7(d)). It was illustrated that Ni was not poisoned by the reactant, and hence, the amount of the absorbed reactant on Ag was reasonably reduced.

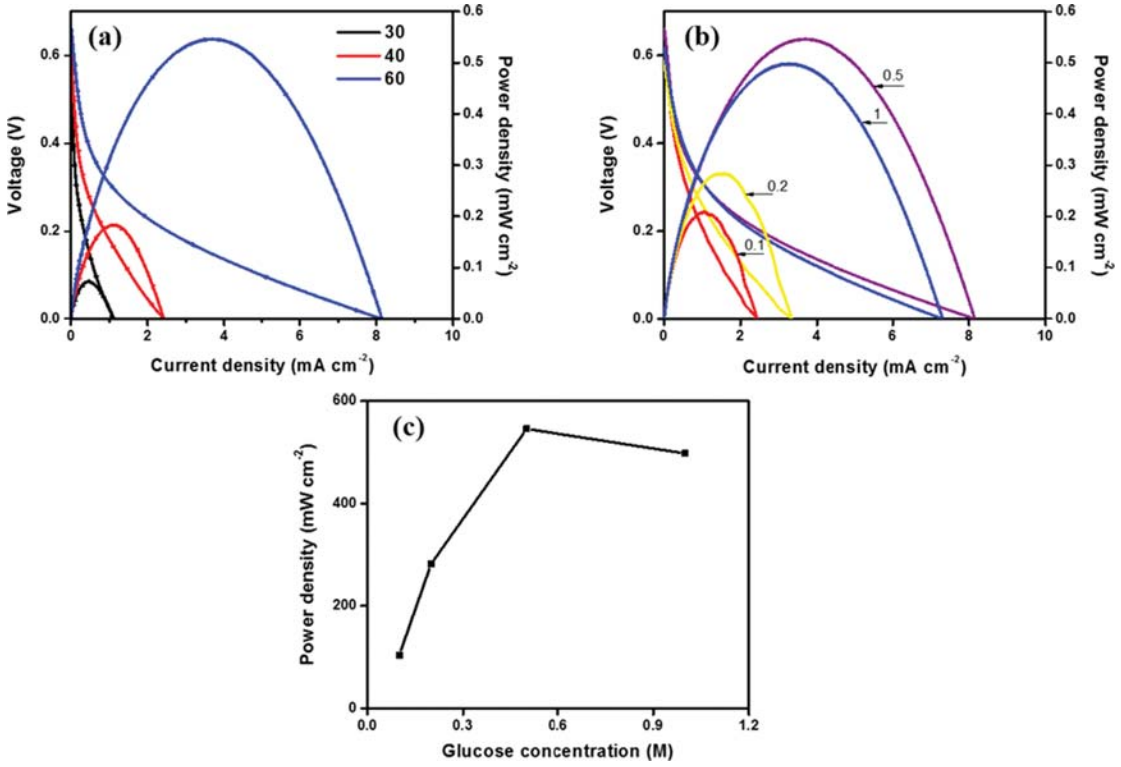

Fig. 8. Power densities of (a) cell in 0.5 M of glucose and 1 M of KOH at operating temperature of 30 °C, 40 °C, 60 °C, (b) cell in various glucose concentrations in 1 M KOH at 60 °C, (c) the comparison of maximum power density with various glucose concentrations.

Consequently, the active sites on Ag were protected for electrocatalytic activities. Finally, gravimetric power density (mW mg^{-1}) of Ag : Ni (1 : 1)@rod graphene was calculated based on the ICP data (Table S1). It delivered an outstanding gravimetric power density of 8 mW mg^{-1} in 0.5 M of glucose and 1.0 M of KOH at an operating temperature of 60 °C.

2-3. Effect of Operating Temperature and Glucose Concentration

Fig. 8 shows the performance of AgNi (1 : 1)-based fuel cell in 0.5 M of glucose and 1 M of KOH aqueous solution in anode and wet air in cathode.

It is clear that temperature positively affects the kinetic property of the electrochemical reaction, and improves the cell performance. For further insight, therefore, it is necessary to examine the effect of operating temperature and glucose fuel cells performance, which are presented in Fig. 8(a). It can be found that the cell performance increases with increasing operating temperature. In particular, the maximum power density of the glucose cell increases from 0.072 mW cm^{-2} to 0.55 mW cm^{-2} when operating temperature increases from 30 °C to 60 °C. The improvement in the cell performance with increasingly operating temperature is due to the accelerated electrochemical kinetics, such as metabolism of the enolization of glucose into enediols [54], and increased conductivity of the hydroxyl ions. Therefore, the operating temperature is an important factor for the cell performance.

The effect of glucose concentration on electrochemical performance was also analyzed. As shown in Figs. 8(b) and 8(c), the electrode of AgNi@rod-grown graphene demonstrates different electrochemical performance based on the concentration of glucose. The power densities increase from 0.104 mW cm^{-2} to 0.55 mW cm^{-2} with the increase in the amount of glucose from 100 mM to 500 mM. However, there was a limitation for glucose concentration, which was 0.5 M of glucose as the maximum. This was because the higher concentration reactant could lead to more violent reactions, and higher current density could cause high voltage loss (such as ohmic loss) and resistance to the delivery of OH ions [55] in the cell unit.

2-4. Effect of Developing 3D Nanostructures on Electrolyte Membrane

Fig. 9 presents an investigation on the distinct preparations of anodic catalysts including the conventional method (AgNi nanoparticle catalysts were deposited on carbon paper and were used as an anode) and the method in which AgNi nanoparticles were deposited on graphene-covered electrolyte membrane.

Both cases show lower performance (0.047 mW cm^{-2}, 0.0075 mW cm^{-2}) compared to the case of AgNi@rod graphene on membrane, which is as about a few ten times (Fig. 7(e)). In fact, power density increases from 0.047 mW cm^{-2} in AgNi conventional cell (Fig. 9(a)) to 0.55 mW cm^{-2} in AgNi@rod graphene/membrane cell due to the enhanced catalytic role by minimizing the size of catalyst nanoparticles by ZnO nanorods. Meanwhile, in the case of AgNi nanoparticles deposited on graphene, as shown in Fig. 9(b), the performance degrades by approximately 73-times compared to that of AgNi@rod graphene on membrane due to the absence of ZnO nanorods. Therefore, the existence of ZnO nanorods may facilitate the transfer of OH^- ions when compared to that of the membrane without ZnO nanorods. In this case, Ag and Ni nanoparticles are deposited directly on the surface of membrane leading to the increase in the ion transfer resistance. Finally, we compared the performance of the as-prepared catalytic electrode with other electrodes, which is shown in Table S2, and the developed catalytic electrode exhibited comparable electrochemical performance. In summary, ZnO nanorods contributed to improving the overall cell performance owing to their high surface area and good catalytic support.

CONCLUSION

Three-dimensional nanostructures were designed as a matrix for the accommodation of metallic nanoparticle catalysts directly on an electrolyte membrane, which enhanced electrochemical reactions in the glucose fuel cell due to large active sites. Ag : Ni (1 : 1)@rod grown on graphene sample showed the best electrochemical performance at 60 °C, which corresponds to a power density of 0.55 mW cm^{-2} (or 8 mW mg^{-1}) at 0.5 M of glucose and 1 M of KOH, even though it utilized low mass loading of catalysts and non-Pt. The AgNi@graphene on membrane developed here, therefore, could promise to open up a new generation of fuel cells to meet an urgent demand for decreasing the usage of catalysts.

ACKNOWLEDGEMENT

This work was supported by the Gachon University research fund

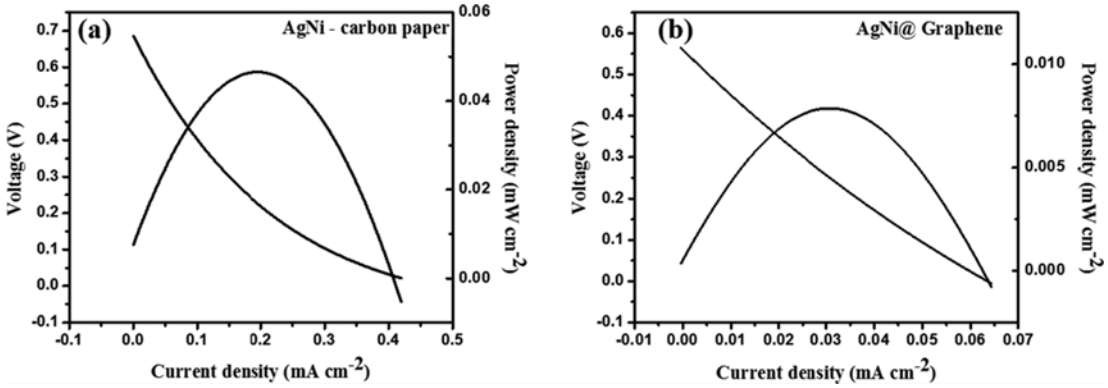

Fig. 9. Power densities of cell in 0.5 M of glucose and 1 M of KOH at operating temperature of 60 °C with (a) AgNi (1 : 1) deposited on a carbon paper anode and (b) AgNi (1 : 1)@ graphene on membrane as anodic electrodes.

of 2018 (GCU-2018-0327) and the Basic Science Research Program of the National Research Foundation of Korea (NRF) and funded by the Ministry of Education (NRF-2016R1D1A1B03934986).

SUPPORTING INFORMATION

Additional information as noted in the text. This information is available via the Internet at http://www.springer.com/chemistry/journal/11814.

REFERENCES

1. S. K. Chaudhuri and D. R. Lovley, *Nat. Biotechnol.,* **21**, 1229 (2003).
2. J. P. Van Wyk, *TRENDS in Biotechnol.,* **19**, 172 (2001).
3. N. Fujiwara, Z. Siroma, T. Ioroi and K. Yasuda, *J. Power Sources*, **164**, 457 (2007).
4. N. Fujiwara, S.-i. Yamazaki, Z. Siroma, T. Ioroi and K. Yasuda, *Electrochem. Commun.*, **8**, 720 (2006).
5. J. Chen, H. Zheng, J. Kang, F. Yang, Y. Cao and M. Xiang, *RSC Adv.*, **7**, 3035 (2017).
6. S. Xu and S. D. Minteer, *ACS Catal.*, **2**, 91 (2012).
7. Y. Zhao, L. Fan, D. Gao, J. Ren and B. Hong, *Electrochim. Acta*, **145**, 159 (2014).
8. Y.-L. Yang, X.-H. Liu, M.-Q. Hao and P.-P. Zhang, *Int. J. Hydrogen Energy*, **40**, 10979 (2015).
9. S. H. Hsieh, M. C. Hsu, W. L. Liu and W. J. Chen, *Appl. Surf. Sci.*, **277**, 223 (2013).
10. J. N. Tiwari, F.-M. Pan, T.-M. Chen, R. N. Tiwari and K.-L. Lin, *J. Power Sources*, **195**, 729 (2010).
11. D. Basu and S. Basu, *Int. J. Hydrogen Energy*, **37**, 4678 (2012).
12. A. Eshghi and M. Kheirmand, *Iranian J. Hydrogen Fuel Cell*, **3**, 11 (2016).
13. C. Hui-Fang, Y. Jian-Shan, L. Xiao, Z. Wei-De and S. Fwu-Shan, *Nanotechnology*, **17**, 2334 (2006).
14. J. Zhu, G. He, L. Liang, Q. Wan and P. K. Shen, *Electrochim. Acta*, **158**, 374 (2015).
15. D. Basu and S. Basu, *Int. J. Hydrogen Energy*, **37**, 4678 (2012).
16. C. A. Apblett, D. Ingersoll, S. Sarangapani, M. Kelly and P. Atanassov, *J. Electrochem. Soc.*, **157**, B86 (2010).
17. N. Fujiwara, S.-i. Yamazaki, Z. Siroma, T. Ioroi, H. Senoh and K. Yasuda, *Electrochem. Commun.*, **11**, 390 (2009).
18. K. Elouarzaki, M. Holzinger, A. Le Goff, J. Thery, R. Marks and S. Cosnier, *J. Mater. Chem. A*, **4**, 10635 (2016).
19. C. H. A. Tsang and D. Leung, *Solid State Sci.*, **71**, 123 (2017).
20. Y. Zhao, X. Liu, X. Wang, P. Zhang and J. Shi, *Int. J. Hydrogen Energy*, **42**, x29863 (2017).
21. S. A. Firdosy, V. A. Ravi, T. I. Valdez, A. Kisor and S. R. Narayan, NASA's Jet Propulsion Laboratory, Pasadena, California (2013).
22. M. Gao, X. Liu, M. Irfan, J. Shi, X. Wang and P. Zhang, *Int. J. Hydrogen Energy*, **43**, 1805 (2018).
23. J. Chen, C. X. Zhao, M. M. Zhi, K. Wang, L. Deng and G. Xu, *Electrochim. Acta*, **66**, 133 (2012).
24. B. Cho, J. Yoon, M. G. Hahm, D.-H. Kim, A. R. Kim, Y. H. Kahng, S.-W. Park, Y.-J. Lee, S.-G. Park and J.-D. Kwon, *J. Mater. Chem. C*, **2**, 5280 (2014).
25. Y. Shao, J. Wang, H. Wu, J. Liu, I. A. Aksay and Y. Lin, *Electroanalysis*, **22**, 1027 (2010).
26. Y. B. Tan and J.-M. Lee, *J. Mater. Chem. A*, **1**, 14814 (2013).
27. F. Bonaccorso, L. Colombo, G. Yu, M. Stoller, V. Tozzini, A. C. Ferrari, R. S. Ruoff and V. Pellegrini, *Science*, **347**, 1246501(2015).
28. H.-J. Choi, S.-M. Jung, J.-M. Seo, D. W. Chang, L. Dai and J.-B. Baek, *Nano Energy*, **1**, 534 (2012).
29. F. Bonaccorso, Z. Sun, T. Hasan and A. Ferrari, *Nat. Photonics*, **4**, 611 (2010).
30. E. Antolini, *Appl. Catal. B: Environ.*, **123**, 52 (2012).
31. H. R. Byon, J. Suntivich and Y. Shao-Horn, *Chem. Mater.*, **23**, 3421 (2011).
32. W. Qian, R. Hao, J. Zhou, M. Eastman, B. A. Manhat, Q. Sun, A. M. Goforth and J. Jiao, *Carbon*, **52**, 595 (2013).
33. H. Baker, In ASM Handbook, Vol. 3 Alloy Phase Diagrams, ASM Int. Mater., 1742 (1992).
34. R. B. McLellan, *Scripta Metallurgica*, **3**, 389 (1969).
35. L. Qu, Y. Liu, J.-B. Baek and L. Dai, *ACS Nano*, **4**, 1321 (2010).
36. C. Xia, Z. Qiao, C. Feng, J.-S. Kim, B. Wang and B. Zhu, *Materials*, **11**, 40 (2018).
37. C. Xia, Z. Qiao, L. Shen, X. Liu, Y. Cai, Y. Xu, J. Qiao and H. Wang, *Int. J. Hydrogen Energy*, **43**, 12825 (2018).
38. W. Hao and Y. Mi, *RSC Adv.*, **6**, 50201 (2016).
39. C. Wang, W. Chen, C. Han, G. Wang, B. Tang, C. Tang, Y. Wang, W. Zou, X.-A. Zhang and S. Qin, *Scientific Reports*, **4**, 4537 (2014).
40. S. M. Kim, A. Hsu, Y.-H. Lee, M. Dresselhaus, T. Palacios, K. K. Kim and J. Kong, *Nanotechnology*, **24**, 365602 (2013).
41. A. Reina, X. Jia, J. Ho, D. Nezich, H. Son, V. Bulovic, M. S. Dresselhaus and J. Kong, *Nano Lett.*, **9**, 30 (2009).
42. A. C. Ferrari, *Solid State Commun.*, **143**, 47 (2007).
43. A. C. Ferrari, J. Meyer, V. Scardaci, C. Casiraghi, M. Lazzeri, F. Mauri, S. Piscanec, D. Jiang, K. Novoselov and S. Roth, *Phys. Rev. Lett.*, **97**, 187401 (2006).
44. L. Malard, M. Pimenta, G. Dresselhaus and M. Dresselhaus, *Phys. Reports*, **473**, 51 (2009).
45. P. Poncharal, A. Ayari, T. Michel and J.-L. Sauvajol, *Phys. Rev. B*, **78**, 113407 (2008).
46. Y. Zhao, W. Li, L. Pan, D. Zhai, Y. Wang, L. Li, W. Cheng, W. Yin, X. Wang, J.-B. Xu and Y. Shi, *Scientific Reports*, **6**, 32327 (2016).
47. Y.-J. Kim, A. Yoon, M. Kim, G.-C. Yi and C. Liu, *Nanotechnology*, **22**, 245603 (2011).
48. Q. Quan, X. Lin, N. Zhang and Y.-J. Xu, *Nanoscale*, **9**, 2398 (2017).
49. K.-L. Ching, G. Li, Y.-L. Ho and H.-S. Kwok, *CrystEngComm*, **18**, 779 (2016).
50. M. Fleischmann, K. Korinek and D. Pletcher, *J. Chem. Soc.*, **7**, 1396 (1972).
51. M. Fleischmann, K. Korinek and D. Pletcher, *J. Electroanal. Chem. Interfacial Electrochem.*, **31**, 39 (1971).
52. C. Zhao, C. Shao, M. Li and K. Jiao, *Talanta*, **71**, 1769 (2007).
53. T. L. Nguyen, D. S. Kim, J. Hur, M. S. Park, S. Yoon and I. T. Kim, *J. Power Sources*, **389**, 28 (2018).
54. Y. Liu, A. Zhang, C. Shen, Q. Liu, X. Cao, Y. Ma, L. Chen, C. Lau, T.-C. Chen, F. Wei and C. Zhou, *ACS Nano*, **11**, 5530 (2017).
55. S. Chaitoglou and E. Bertran, *J. Mater. Sci.*, **52**, 8348 (2017).

Supporting Information

AgNi@ZnO nanorods grown on graphene as an anodic catalyst for direct glucose fuel cells

Thoa Thi Kim Huynh[*,‡], Thao Quynh Ngan Tran[,‡], Hyon Hee Yoon[*], Woo-Jae Kim[***,†], and Il Tae Kim[*,†]**

*Department of Chemical and Biological Engineering, Gachon University, Seongnam-si, Gyeonggi-do 13120, Korea
**Department of Machine and Equipment, Faculty of Chemical Engineering,
Industrial University of Ho Chi Minh City, No 12 Nguyen Van Bao, Go Vap, HCMC, Vietnam
***Department of Chemical Engineering and Materials Science, Ewha Womans University, Seoul 03760, Korea
(*Received 12 March 2019 • accepted 7 May 2019*)

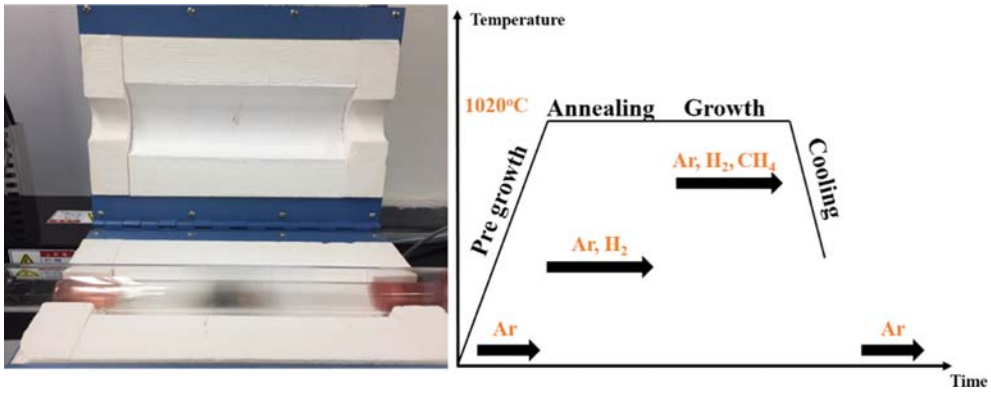

Fig. S1. Image of practical CVD system and experimental process.

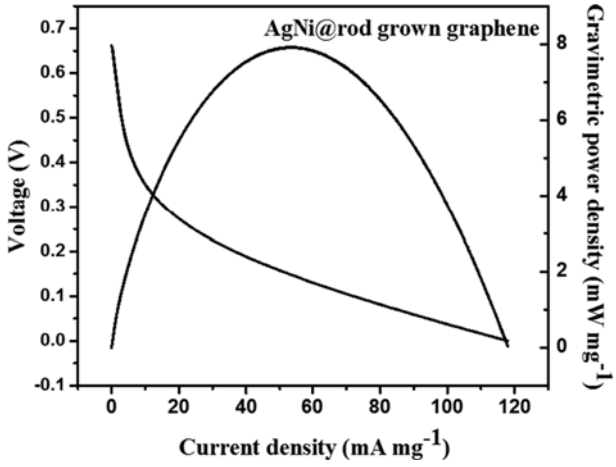

Fig. S2. Gravimetric power density (mW g^{-1}) of AgNi@rod grown-graphene in 0.5 M of glucose and 1 M of KOH at operating temperature of 60 °C. It generates a gravimetric power density of 8 mW mg^{-1}.

Table S1. ICP data of Ag and Ni elements on the electrode of AgNi@rod grown on graphene

Element	Ni	Ag
Concentration (mmol/l)	0.00022	0.00030

ICP measurement: The sample of AgNi@rod grown on graphene was dissolved in 15 ml of acidic solution. The obtained solution was then diluted 100 times by DI water. 1 ml of the solution was taken for ICP test

Table S2. Comparison on power densities with different catalytic electrodes for DGFC

Anode			Results		Ref.
Catalyst	Fuel	Loading	OCV [V]	Power density [mW cm^{-2}]	
Au/C	Glucose	1.2 mg	0.85	0.86	[1]
Au/MnO_2-C	Glucose	0.6 mg	0.86	1.1	[1]
Nano porous Au- PtBi	Glucose	0.45 mg	0.90	8	[2]
PtAu/C	Glucose	0.45 mg	0.90	0.72	[3]
AgNi/ ZnO nRs-graphene	Glucose	0.069 mg	0.64	0.55	This work

REFERENCES

1. L. Li, K. Scott and E. H. Yu, *J. Power Sources*, **221**, 1 (2013).
2. H. Guo, H. Yin, X. Yan, S. Shi, Q. Yu, Z. Cao and J. Li, *Scientific Reports*, **6**, 39162 (2016).
3. D. Basu, S. Sood and S. Basu, *Chem. Eng. J.*, **228**, 867 (2013).